Int. J. Electrochem. Sci., 8 **(2013)** 4234 - 4259

International Journal of
ELECTROCHEMICAL
SCIENCE
www.electrochemsci.org

Charge Transfer Complexes as a Semiconductor Models: Outline of Spectroscopic Studies on Electron Donor-Acceptor Complexes of Hexane-1,6-diol with Different π-Acceptors

Moamen S. Refat[1,2,*], *Mohamed Y. El-Sayed*[3], *Abdel Majid A. Adam*[1] , *Hosam A. Saad*[1,3] *and Hala H. Eldaroti*[4]

[1] Chemistry Department, Faculty of Science, Taif University, 888 Taif, Saudi Arabia
[2] Chemistry Department, Faculty of Science, Port Said University, Egypt
[3] Chemistry Department, Faculty of Science, Zagazig University, Zagazig, Egypt
[4] Chemistry Department, Faculty of Education, Alzaeim Alazhari University, Khartoum, Sudan
[*]E-mail: msrefat@yahoo.com

Received: 29 January 2013 / *Accepted:* 21 February 2013 / *Published:* 1 March 2013

Electron donor-acceptor complexes (CT-complexes) formed between hexane-1,6-diol (hexol) as a donor with quinol ($Q(OH)_2$), picric acid (PA), 1,3-dinitrobenzene (DNB), chloranilic acid (CLA) and *p*-chloranil (CHL) as a π-acceptors have been synthesized and spectroscopically studied in methanol as a solvent at room temperature. Based on the elemental analyses and photometric titrations, the stoichiometry of CT complexes formed with $Q(OH)_2$, PA, CLA and CHL as acceptors are found to be 1:2 ratio, but with DNB acceptor is found to be 1:1 ratio. Benesi-Hildebrand and its modification methods were applied to estimate the spectroscopic and physical data. The spectroscopic techniques such as (IR, ^{1}H-NMR, and UV-vis) spectra and elemental analyses (C,H,N) as well as thermogravimetric analysis (TG) were used to characterize the chelating behavior of the five hexol synthetic CT complexes. The kinetic thermodynamic parameters such as, activation energy, E^*, enthalpy, ΔH^*, entropy, ΔS^*, and Gibbs free energy, ΔG^*, have been calculated from TG curves, using Coats-Redfern and Horowitz-Metzger methods. The hexol CT-complexes were antimicrobial assessed against two kinds of bacteria and fungi species. The results show that, hexol complexes which have high energy gap values (HOMO-LUMO) exhibit good antibacterial activity against all bacteria species under investigation, and only hexol/$Q(OH)_2$ and hexol/PA complexes which possess highest energy gap value exhibit a good antifungal activity against *Candida albicans*. These results reveal that the energy gap reflects the chemical and biological activity of the charge transfer complex.

Keywords: Charge transfer complexes, Hexane-1,6-diol, biological evaluation, HOMO and LUMO.

1. INTRODUCTION

The term charge transfer complex (CTC) was introduced firstly by Mulliken [1-2], and discussed widely by Foster [3]. Mulliken aimed to define a new type of adduct to explain the behavior of certain classes of molecules, which do not conform to classical patterns of ionic, covalent, and coordination of hydrogen bonding components. While such adducts largely retain some of the propertied of the components, some changes are apparent, e.g. its solubility, the diamagnetic and paramagnetic susceptibility. Other differences have also been found with electrochemical techniques. Some complexes can be isolated as crystals of regular stoichiometry and structure. One feature of charge transfer complexes is that the association constant of the complex decreases with increasing temperature. The effect is due to the thermal motion disorienting the partners of the complex. Mulliken [4,5] also showed that the charge transfer interactions within a molecular complex consisting of an electron donor D and an electron acceptor A involved a resonance with a transfer of charge from D to A:

$$D + A \leftrightarrows D^{+}A^{-} \leftrightarrows D^{+} + A^{-}$$

Charge transfer complexation is currently achieve the great importance in biochemical, bioelectrochemical energy transfer process [6], biological systems [7], and drug-receptor binding mechanism, for examples, drug action, enzyme catalysis, ion transfers through lipophilic membranes [8], and certain π-acceptors have successfully been utilized in pharmaceutical analysis of some drugs in pure form or in pharmaceutical preparations [9-15]. Recently, many studies have been widely reported about the rapid interactions between different kinds of drugs and related compounds as donors like morpholine, norfloxacin, ciprofloxacin, and sulfadoxine, with several types of σ and π-electron acceptors [16-30]. On the other hand, electron donor-acceptor (EDA) interaction has a worth attention for chemical reactions like addition, substitution and condensation [31,32]. It shows a great important in many application topics and fields, like in non-liner optical materials and electrical conductivities [33-36], second order non-liner optical activity [37], micro emulsion [38], surface chemistry [38], photo catalysts [39], dendrimers [40], solar energy storage [41], organic semiconductors [42], as well as in studying redox processes [43]. Charge transfer complexes using organic species are intensively studied because of their special type of interaction, which is accompanied by the transfer of an electron from the donor to the acceptor [44,45]. In addition, protonation of the donor from acidic acceptors is generally a route for the formation of ion pair adducts [46-48].

Herein, this paper describes the comprehensive studies on the formation of CT-complexes which formed between hexane-1,6-diol as a donor with five π-acceptors; quinol ($Q(OH)_2$), picric acid (PA), dinitrobenzene (DNB), chloranilic acid (CLA), and *p*-chloranil (CHL). The nature and structure of the final products both in solution and solid phase have been characterized to interpret the behavior of interactions using elemental analysis, infrared (IR), ^{1}H-NMR and electronic spectra. The spectroscopic, physical data were analyzed in terms of formation constant (K_{CT}), molar extinction coefficient (ε_{CT}), standard free energy ($\Delta G°$), oscillator strength (f), transition dipole moment (μ), resonance energy (R_N) and ionization potential (I_D). The thermal behavior of the obtained complexes as

well as kinetic thermodynamic parameters (E^*, ΔS^*, ΔH^* and ΔG^*) have also been investigated. Finally, antimicrobial activity of hexol complexes was tested against different Gram (+) and Gram (-) bacteria species such as, *Staphylococcus aureus* (*S. aureus*), *Bacillus subtilis*, *Escherichia coli* (*E. coli*) and *Pseudomonas aeuroginosa* (*P. aeuroginosa*), and antifungal screening was studied against two species, *Aspergillus flavus* and *Candida albicans*.

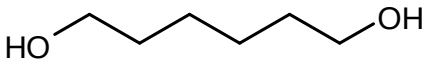

Donor

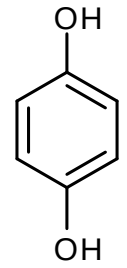

$Q(OH)_2$

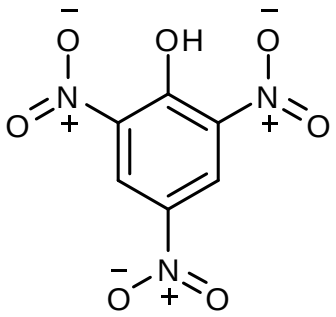

PA

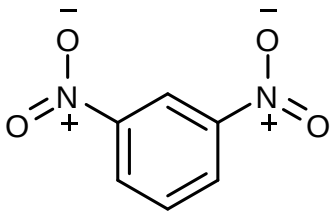

DNB

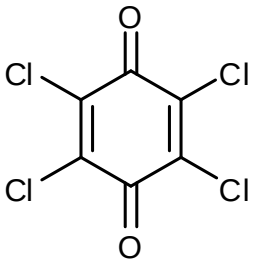

p-CHL

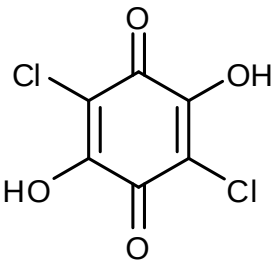

CLA

Formula I. Structure of hexol donor and π-acceptors.

2. EXPERIMENTAL

2.1 Materials

Hexane-1,6-diol (hexol) (MF=$C_6H_{14}O_2$) and π-acceptors were of analytical reagent grade (Merck Company) and used without any further purification. The structures of hexol and π-acceptors are presented in Formula I.

2.2 Synthesis of hexol CT-complexes

The solid CT-complexes of hexol with acceptors; $Q(OH)_2$, PA, DNB, CLA, and CHL were prepared by mixing 1 mmole of the hexol as a donor in methanol (20 ml) with 2 mmole of each acceptor in the same solvent. The mixtures were stirred at room temperature for 1 h, precipitated the solid CT-complexes. The solid precipitates were filtered off, washed several times with little amounts of methanol, and then dried under vacuum over anhydrous calcium chloride.

2.3 Photometric titration measurements

The photometric titrations measurements were performed for the reactions of the donor with $Q(OH)_2$, PA, DNB, CLA, and CHL at 293, 355, 235, 305, and 289 nm, respectively. A 0.25, 0.50, 0.75, 1.00, 1.50, 2.0, 2.50, 3.00, 3.50 and 4.00 mL aliquot of a standard solution (5.0×10^{-4} M) of the appropriate acceptor in MeOH was added to 1.00 ml of 5.0×10^{-4} M hexol also in MeOH. The total volume of the mixture was 5 mL. The concentration of hexol (C_d) in the reaction mixture was kept fixed at 5.0×10^{-4} M whiles the concentration of the π-acceptors (C_a) changed over a wide range of concentrations from 0.25×10^{-4} M to 4.00×10^{-4} M, to produce solution in each case of donor: acceptor molar reaction varying from 4:1 to 1:4. The stoichiometry of the molecular CT-complexes was determined by the application of the conventional spectrophotometric molar ratio according to the known methods [49] through the plot of the absorbance of each CT-complex as a function with the ratio of (C_d): (C_a). The Benesi-Hildebrand and its modification plots were obtained [50,51] in order to calculate the formation constant, K_{CT}, and the absorpativity, ε_{CT}, values for each CT-complex resulted from this study.

2.4 Instrumentation and physical measurements

The electronic absorption spectra of the donor, acceptors and the resulted CT-complexes were recorded in the region of (800-200 nm) by using a Perkin-Elmer Lambda 25 spectrophotometer with a 1 cm quartz cell. The mid infrared spectra (IR) measurements (KBr discs) of the solid CT-complexes were carried out on a Genesis II FT-IR spectrophotometer in the υ= 4000-400 cm^{-1} range. ^{1}H-NMR spectra were obtained on a Bruker DRX-250 spectrometer, operating at 250.13 MHz using a dual 5 mm probe head. The measurements were carried out at ambient temperature using DMSO-d_6 as the solvent and TMS as an internal reference. ^{1}H-NMR data are expressed in parts per million (ppm), referenced internally to the residual proton impurity in DMSO solvent. Thermogravimetric measurements (TGA) were carried out in the temperature range 25-800 °C in nitrogen atmosphere using a using a Shimadzu TGA –50H thermal analyzers. The experimental conditions were aluminum crucible with a definite mg of sample, dynamic nitrogen atmosphere (nitrogen flow 30 ml/min.) and heating rate of 10 °C/min. The elemental analyses of carbon, hydrogen and nitrogen contents were performed by the microanalysis unit at Cairo University, Egypt, using a Perkin-Elmer CHN 2400 (USA).

2.5 Antimicrobial investigation

Antimicrobial activity of the hexol CT- complexes as well as the pure solvent was determined using a modified Bauer-Kirby disc diffusion method [52], against different Gram (+) and Gram (-) bacteria species; *Staphylococcus aureus*, *Bacillus subtilis*, *Escherichia coli* and *Pseudomonas aeuroginosa*, and antifungal screening was studied against two species, *Aspergillus flavus* and *Candida albicans*. The microanalysis unit at Cairo University, Egypt performed the investigations. For these investigations, briefly, 100 μl of the test bacteria/fungi were grown in 10 ml of fresh media until they reached a count of approximately 108 cells/ml for bacteria or 105 cells/ml for fungi [53]. 100 μl of microbial suspension was spread onto agar plates. The nutrient ager medium for antibacterial was (0.5% Peptone, 0.1% Beef extract, 0.2% Yeast extract, 0.5% NaCl and 1.5% Agar-Agar) and for antifungal (3% Sucrose, 0.3% $NaNO_3$, 0.1% K_2HPO_4, 0.05% KCl, 0.001% $FeSO_4$, 2% Agar-Agar) [54]. Isolated colonies of each organism that might be playing a pathogenic role were selected from primary agar plates and tested for susceptibility. Disc diffusion method for filamentous fungi tested by using developed standard method (M38-A) [55], where disc diffusion method for yeast tested by developed standard method (M44-P) [56]. Plates inoculated with filamentous fungi, bacteria and yeast were incubated at 25 °C, 35-37 °C and 30 °C, respectively. After incubation for 48 h, the inhibition (sterile) zone diameters (including disc) were measured with slipping calipers of the National Committee for Clinical Laboratory standards (NCCLS, 1993) [57], and expressed in mm. Standard discs of Tetracycline (Antibacterial agent) and Amphotericin B (Antifungal agent) served as positive controls for antimicrobial activity, where filter discs impregnated with 10 μl of DMSO solvent were used as a negative control. An inhibition zone diameter over 8 mm indicates that the tested compounds are active against some of bacteria and fungi under investigation. The concentration of each solution was $1.0x10^{-3}$ mol dm^{-3}. Commercial DMSO was employed to dissolve the tested samples.

3. RESULTS AND DISCUSSION

3.1 Elemental analysis

The elemental analysis data (C, H, and N) of the hexol CT-complexes were performed and the obtained results as follow;

1 [(hexol)$(Q(OH)_2)_2$]; $C_{18}H_{26}O_6$; Mol. wt. = 338; Calc.: %C, 63.90; %H, 7.69, Found: %C, 63.26; %H, 7.10

2 [(hexol)$(PA)_2$]; $C_{18}H_{20}O_{16}N_6$; Mol. wt. = 576; Calc.: %C, 37.50; %H, 3.47; %N, 14.58, Found: %C, 37.31; %H, 3.30; %N, 14.43

3 [(hexol)(DNB)]; $C_{12}H_{18}O_6N_2$; Mol. wt. = 286; Calc.: %C, 50.35; %H, 6.29; %N, 9.79, Found: %C, 49.32; %H, 6.37; %N, 9.25

4 [(hexol)$(CLA)_2$]; $C_{18}H_{18}O_{10}Cl_4$; Mol. wt. = 536; Calc.: %C, 40.30; %H, 3.36, Found: %C, 40.17; %H, 3.54

5 [(hexol)$(CHL)_2$]; $C_{18}H_{14}O_6Cl_8$; Mol. wt. = 610; Calc.: %C, 37.41; %H, 2.50, Found: %C, 37.45; %H, 2.76

It can be seen that the resulted values agree quite well with the calculated values, and the suggested values are matched with the molar ratio introduced from the photometric titration curves.

3.2 Determination of formation constant (K_{CT}) and molar extinction coefficient (ε_{CT})

The 1:1 modified Benesi-Hildebrand equation [50] was used in the calculations of the hexol-DNB charge transfer complex;

$$(C_aC_d)/A = 1/K\varepsilon + (C_a + C_d)/\varepsilon \quad (1)$$

where C_a and C_d are the initial concentrations of the acceptor and the donor, respectively, and A is the absorbance of the strong band at nm. When the $(C_aC_d)/A$ values for 1:1 charge transfer complex are plotted against the corresponding $(C_a + C_d)$ values, straight line is obtained with a slope of $1/\varepsilon$ and intercept of $1/K\varepsilon$.

The spectrophotometric titrations of the intermolecular charge transfer complexes formed from the reactions of hexol with $Q(OH)_2$, PA, CLA, and CHL acceptors refereed to the formation of 1:2 CT complexes. The 1:2 Eq. (2) [51] was used in the calculations;

$$(C_a)^2C_d/A = 1/K\varepsilon + 1/\varepsilon C_a\,(4C_d + C_a) \quad (2)$$

where C_a and C_d are the initial concentration of the acceptor ($Q(OH)_2$, PA, CLA and CHL) and hexol, respectively, and A is the absorbance of the detected CT-band. The data obtained C_a, C_d, $(C_a)^2C_d$, $C_a(4C_d+C_a)$ and $(C_a)^2C_d/A$ in methanol were calculated. By plotting $(C_a)^2C_d/A$ values vs. C_a $(4C_d+C_a)$, straight lines are obtained with a slope of 1/ε and an intercept of 1/Kε.

The data resulted (Table 1) shows that the hexol/A (where A: $Q(OH)_2$, PA, CLA, and CHL) systems give high values of both formation constant (K_{CT}) and molar absorptivity (ε_{CT}). This high value of (K_{CT}) reflects the high stability of the CT-complexes.

3.3 Determination of the spectroscopic and physical data of the hexol CT- complexes

The spectroscopic and physical data such as formation constant (K_{CT}), molar extinction coefficient (ε_{CT}), standard free energy ($\Delta G°$), oscillator strength (f), transition dipole moment (μ), resonance energy (R_N), and ionization potential (I_P), were estimated in methanol at 25 °C. The calculations can be summarized as follow;

From the CT absorption spectra, the oscillator strength f can be estimated by using the approximate formula [58];

$$f = 4.319\times10^{-9}\int\varepsilon_{CT}\,d\nu \quad (3)$$

where $\int \varepsilon_{CT}\, d\nu$ is the area under the curve of the extinction coefficient of the absorption band in question vs. frequency. To a first approximation;

$$f = 4.319\times10^{-9}\, \varepsilon_{CT}\, \nu_{½} \quad (4)$$

where ε_{CT} is the maximum extinction coefficient of the CT-band and $\nu_{½}$ is the half bandwidth in cm^{-1}, i.e., the width of the band at half of the maximum extinction. The observed oscillator strength values of the CT bands are given in Table 1. The transition dipole moment (μ) of the hexol CT-complexes, Table 1, have been calculated from Eq. (5) [59];

$$\mu \text{ (Debye)} = 0.0958\, [\varepsilon_{CT}\nu_{½}/\nu_{max}]^{½} \quad (5)$$

The transition dipole moment is useful for determining if transitions are allowed, that the transition from a bonding π orbital to an antibonding π^* orbital is allowed because the integral defining the transition dipole moment is nonzero. The ionization potential (I_P) of the hexol donor in their charge transfer complexes were calculated by using empirical equation derived by Aloisi and Pignataro Eq. (6) [60];

$$I_P\,(eV) = 5.76 + 1.53\times10^{-4}\nu_{CT} \quad (6)$$

where ν_{CT} is the wave number in cm^{-1} corresponding to the CT band formed from the interaction between donor and acceptor. The electron donating power of a donor molecule is measured by its ionization potential which is the energy required to remove an electron from the highest occupied molecular orbital. Briegleb and Czekalla [61] theoretically derived the relation to obtain the resonance energy (R_N) given as below;

$$\varepsilon_{CT} = 7.7\times10^{-4}/\,[h\nu_{CT}/[R_N]\text{-}3.5] \quad (7)$$

where ε_{CT} is the molar absorptivity coefficient of the CT-complex at the maximum of the CT absorption, ν_{CT} is the frequency of the CT peak and R_N is the resonance energy of the complex in the ground state, which, obviously is a contributing factor to the stability constant of the complex (a ground state property). The values of R_N for the complexes under study have been given in Table 1. The energy (E_{CT}) of the π-π^* interaction between donor (hexol) and acceptors, was calculated by using the equation derived by Briegleb [62];

$$E_{CT} = (h\nu_{CT}) = (1243.667/\lambda_{CT}) \quad (8)$$

where λ_{CT} is the wavelength of the CT band. The calculated values of E_{CT} are given in Table 1. The standard free energy changes of complexation ($\Delta G°$) were calculated from the formation constant by using the equation derived by Martin et al. [63];

$$\Delta G^{\circ} = -2.303RT \log K_{CT} \quad (9)$$

where ΔG° is the free energy change of the CT-complexes (kJmol^{-1}), R is the gas constant (8.314 Jmol^{-1}K), T is the temperature in Kelvin degrees (273+ °C) and K_{CT} is the formation constant of the complex (Lmol^{-1}) at room temperature.

Table 1. Spectrophotometric results of the hexol CT-complexes.

Complex	λ_{max} (nm)	E_{CT} (eV)	K (Lmol^{-1})	ε_{max} (Lmol^{-1}cm^{-1})	f	μ	I_p	R_N	ΔG° (kJmol^{-1})
hexol/Q(OH)$_2$	293	4.24	4.74×10^7	6.57×10^4	47.30	54.27	10.98	0.91	43,796
hexol/PA	355	3.50	6.94×10^7	9.29×10^4	40.12	55.02	10.07	0.81	44,743
hexol/DNB	235	5.29	4.65×10^4	5.00×10^4	28.79	37.90	12.27	1. 51	38,041
hexol/CLA	305	4.08	8.46×10^7	7.43×10^4	32.09	45.61	10.78	0.90	45,232
hexol/CHL	289	4.30	6.61×10^7	7.28×10^4	41.92	50.74	11.05	0.94	44,622

3.4 Spectroscopic characterization of CT-complexes

The electronic absorption spectra of hexol, π-acceptors (Q(OH)$_2$, PA, DNB, CLA and CHL) and the formed CT-complexes are shown in Fig. 1.The spectra demonstrate that the formed CT-complexes have strong absorption bands at 293, 355, 235, 305 and 289 nm for [(hexol)(Q(OH)$_2$)], [(hexol)(PA)$_2$], [(hexol)(DNB)], [(hexol)(CLA)$_2$] and [(hexol)(CHL)$_2$] complex, respectively. The peak absorbances appeared in the spectra that assigned to the formed CT complexes were measured and plotted as function of the ratio C_d: C_a according to the known method. The formation constant (K) and molar absorptivity (ε) for [(hexol)(DNB)] complex were calculated by applying the 1:1 Benesi-Hildebrand Eq. (1), where, the 1:2 modified Benesi-Hildebrand Eq. (2), was used in calculating for the complexes of Q(OH)$_2$, PA, CLA and CHL acceptors. The modified Benesi-Hildebrand plots are given in Fig. 2, where the data obtained throughout these calculations are given in Table 1. This Table have the calculated values of the spectroscopic data like; ε, K, μ, R_N, ΔG, I_P and f, which deduced from Eqs. (3)-(9). Generally, these complexes show high values of both the formation constant (K) and the extinction coefficients (ε). These high values of K confirm the expected high stabilities of the formed CT-complexes as a result of the expected high donation of the hexol. The equilibrium constants are strongly dependent on the nature of the used acceptor including the type of electron withdrawing substituents to it such as nitro and halo groups [64]. For example, the value of equilibrium constant for [(hexol)(CLA)$_2$] is the highest value than other complexes. This value is about twice times higher than the value of equilibrium constant for the complex [(hexol)(Q(OH)$_2$)$_2$], reflecting the relatively higher powerful electron acceptance ability for CLA.

3.4.1 [(hexol)(Q(OH)$_2$)] complex

The full IR spectrum of the [(hexol)(Q(OH)$_2$)] CT-complex is shown in Fig. 3. The stretching of O-H of both hexol and Q(OH)$_2$ show a drastic shift to lower frequencies and increasing in the intensities of vibration motions, which indicated that the interaction placed among the –OH group of Q(OH)$_2$ and –OH group of hexol through the hydrogen bonding detected within region 3000-2000 cm^{-1}. Also the stretching of C-O of hexol and Q(OH)$_2$ show a drastic shift to lower frequencies and decreasing the intensities upon complexation. These shifts are resulted from building of higher charge density on the hydrogen bond between donor and acceptor. According to these observations, the suggested structure of hexol/Q(OH)$_2$ complex is presented in Formula II.

^{1}H-NMR (CDCl$_3$) for symmetrical hexane-1,6-diol-di(benzene-1,4-diol), gave a signals at (Fig. 4): ^{1}H-NMR (DMSO-d$_6$, δ ppm): δ = 2.23 (t, 4H, 2(C$\underline{H}_2$CH$_2$CH$_2$-OH)$_2$, 2.58 (m, 4H, 2(CH$_2$C$\underline{H}_2$CH$_2$-OH)$_2$), 2.82 (s, 2H, 2OH(CH$_2$OH)$_2$), 3.25 (s, 2H, 2OH, hydrogen bonded), 3.38 (t, 4H, 2(CH$_2$CH$_2$C$\underline{H}_2$OH)$_2$), 6.62 (s, 8H, Ar-H), 7.74 (s, 2H, Ar-OH). The ^{1}H-NMR showed that the three main signals at 1.44, 1.57 and 2.42 ppm in the free hexol due to aliphatic protons of CH$_2$ (8H) and protons of hydroxyl group (2H) were downfield shifted, indicating the involvement of the CH$_2$-OH groups in complxation. These displacement due to the increase of the shielding of these protons with overall decrease in the value of the coupling constant because of the change of the magnetic environment of all protons as a result of complex formation. The ^{1}H-NMR spectrum also shows signals at δ= 6.62 and 7.74 for eight aromatic quinol protons and two quinol OH protons, respectively.

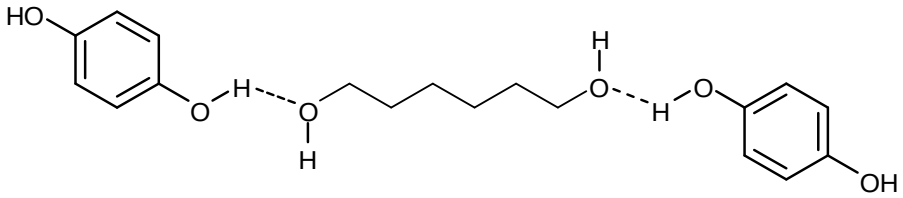

Formula II. Suggested structure of [(hexol) (Q(OH)$_2$)$_2$] complex.

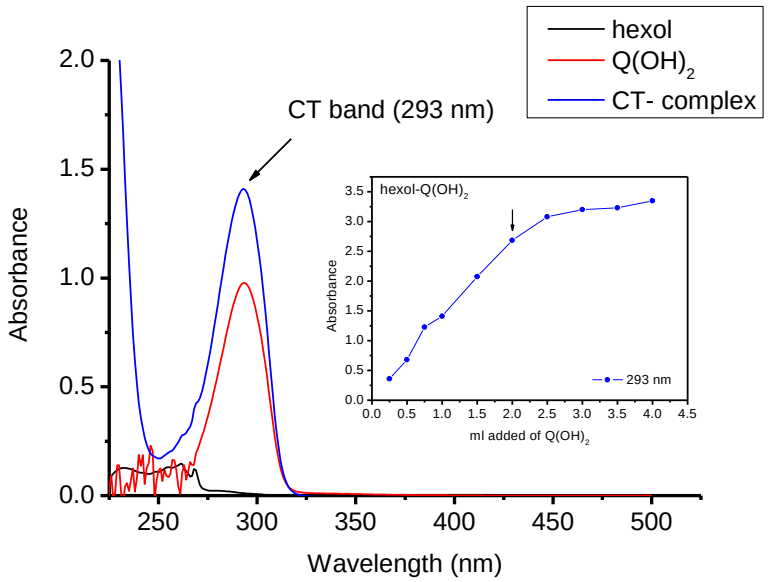

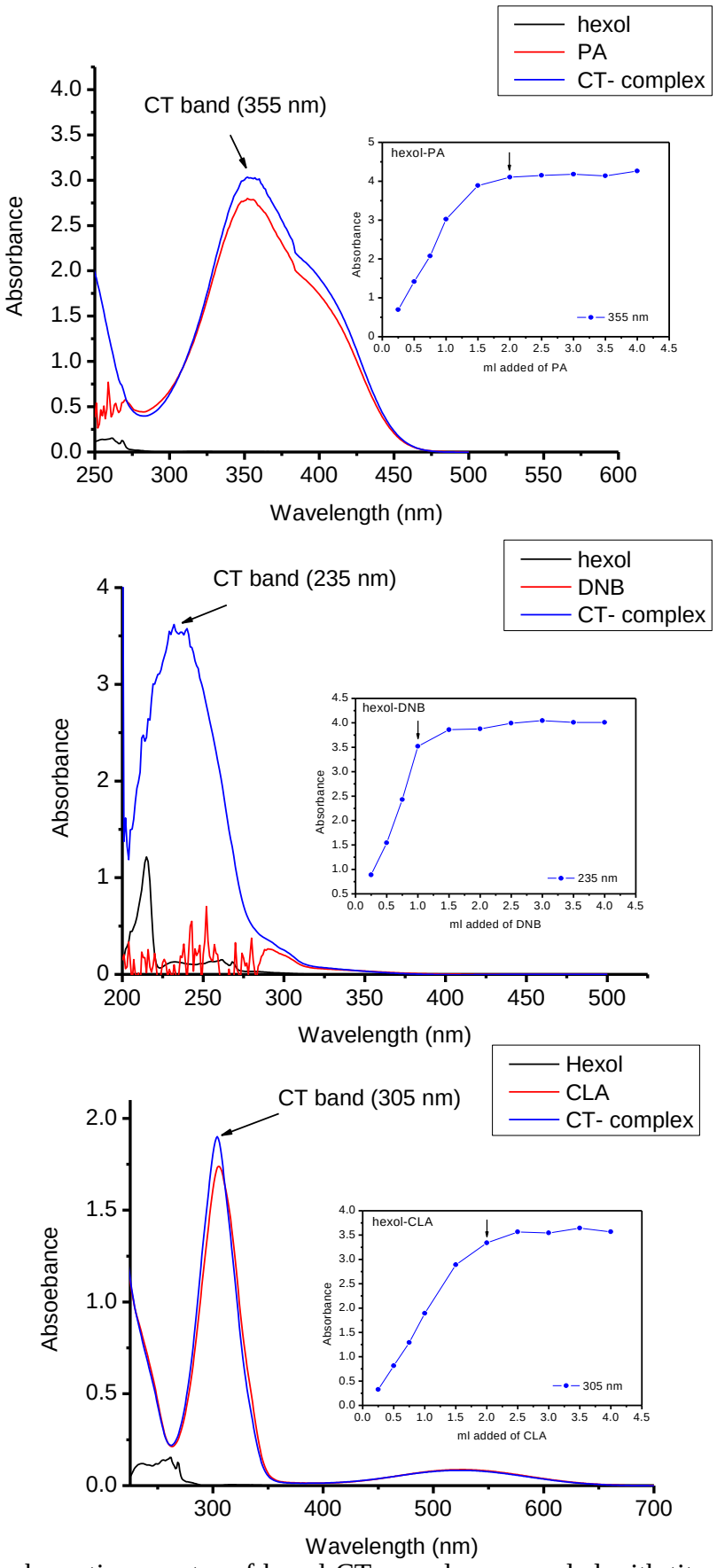

Figure 1. Electronic absorption spectra of hexol CT-complexes coupled with titration spectra of each system at the detectable peak.

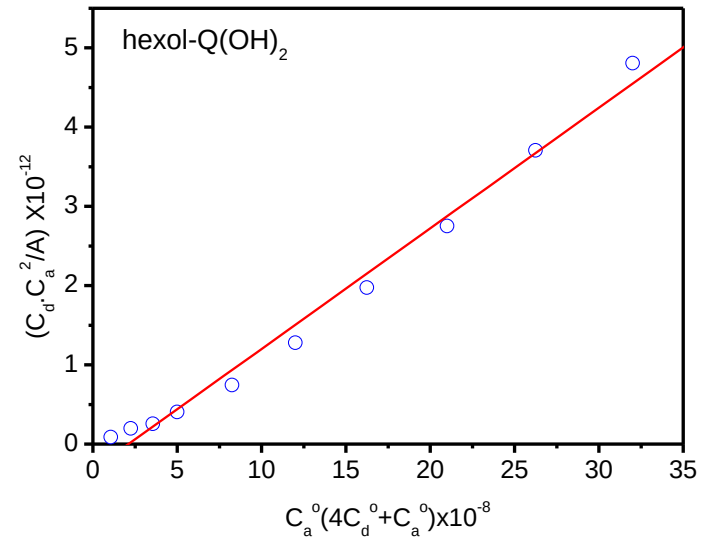
hexol-Q(OH)2
(Cd.Ca2/A) X10-12
Ca°(4Cd°+Ca°)x10-8
0
1
2
3
4
5
0
5
10
15
20
25
30
35

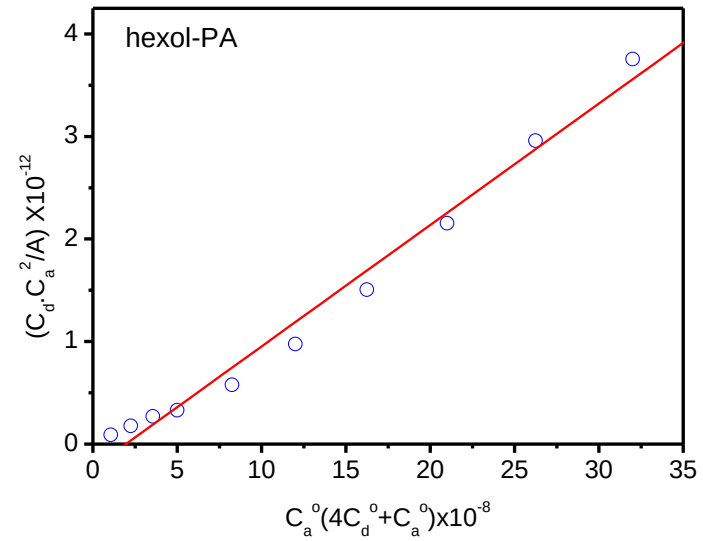
hexol-PA
(Cd.Ca2/A) X10-12
Ca°(4Cd°+Ca°)x10-8
0
1
2
3
4
0
5
10
15
20
25
30
35

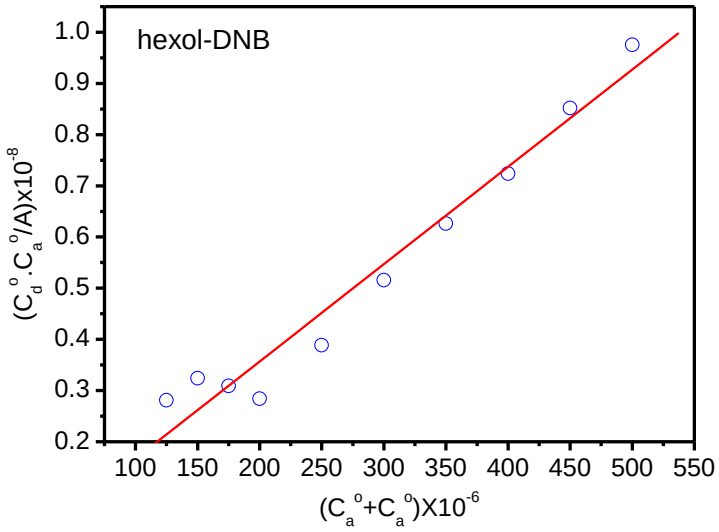
hexol-DNB
(Cd°.Ca°/A)x10-8
(Ca°+Ca°)X10-6
0.2
0.3
0.4
0.5
0.6
0.7
0.8
0.9
1.0
100
150
200
250
300
350
400
450
500
550

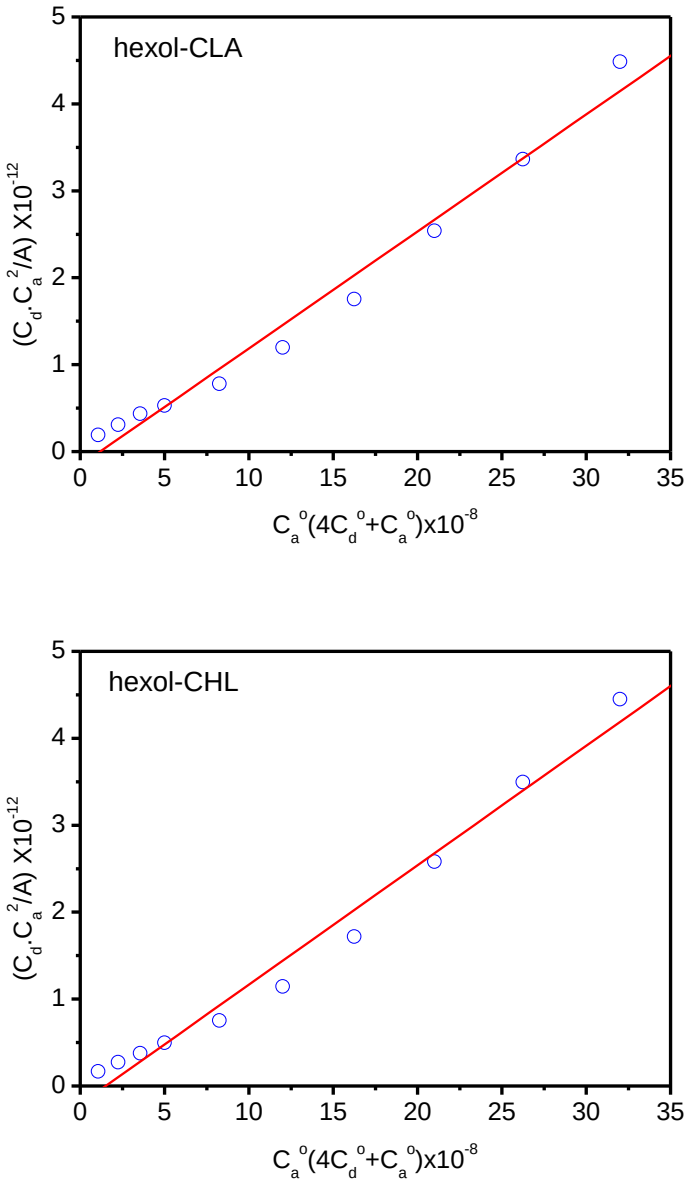

Figure 2. The modified Benesi-Hildebrand plots of hexol-$Q(OH)_2$, hexol-PA, hexol-DNB, hexol-CLA and hexol-CHL systems at detectable peaks of 293, 355, 235, 305 and 289 nm, respectively.

3.4.2 [(hexol)$(PA)_2$] complex

The full spectrum of this CT-complex is shown in Fig. 3. The OH stretching vibration band in hexol was shifted and decreased in the CT complex. This shifted band is attributed to the stretching vibration of the intermolecular hydrogen bond [65]. This result caused to the protonation of the $^+$OH group of the donor from two sides, through protons transfer from the acidic center of the PA acceptor under the acid-base theory. The shift of the IR bands of the acceptor to lower wavenumbers reflects a donor to acceptor charge transfer of n$\rightarrow \pi^*$ interaction, $D_{HOMO} \rightarrow D_{LUMO}$ transition [66]. The hydrogen bonding between the hexol donor and PA acceptor can be formulated as formula III.

^{1}H-NMR ($CDCl_3$) for symmetrical hexane-1,6-diol-di(2,4,6-trinitrophenol), gave signals at (Fig. 4): ^{1}H-NMR (DMSO-d_6, δ ppm): δ = 1.64 (t, 4H, 2($C\underline{H}_2CH_2CH_2$-OH), 2.60 (m, 4H, 2($CH_2C\underline{H}_2CH_2$-OH)), 2.88 (s, 2H, 2OH(CH_2OH)), 3.03 (t, 4H, 2($CH_2CH_2C\underline{H}_2$OH)), 8.00 (s, 4H, Ar-H), 8.80 (s, 2H, Ar-OH, hydrogen bonded). The ^{1}H-NMR showed that the two signals at 1.44 and 1.57 ppm in the free hexol, which assigned to aliphatic proton (8H) were downfield shifted, this shift is due to the CT-complex formation. The peak observed at 8.80 ppm in the complex is due to the formation of hydrogen bonding between picric acid and hexol, because in free picric acid the peak at δ= 11.94 ppm is due to the –OH proton of picric acid [67] which is absent in the spectrum of CT-complex. The ^{1}H-NMR confirm that the reaction between hexol and PA carried out in 1:2 ratio through formation of hydrogen bond between the hydroxyl group of hexol and phenolic group of PA.

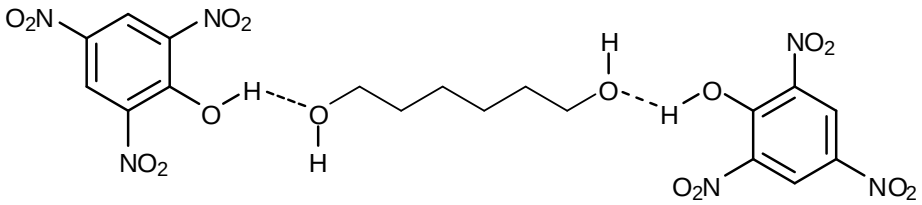

Formula III. Suggested structure of [(hexol) $(PA)_2$] complex.

3.4.3 [(hexol)(DNB)] complex

A comparison of the relevant IR spectral bands of the free donor, hexol, and DNB acceptor with corresponding appeared in the IR spectrum of the isolated CT complex, clearly indicated that the characteristic bands of hexol (ν(-OH); 3392 and 3323 cm^{-1}) show critical decreasing in intensity. This could be attributed to the expected electronic structure changes upon the formation of the CT-complex. The assumption place of CT-interaction between hexol and DNB comes through the ability of hydrogen centered between two with-drawing nitro groups to form hydrogen bonding with one of –OH groups of hexol. Thus it may conclude that the molecular complexes are formed through $n\rightarrow\pi^*$ charge migration from HOMO of the donor to the LUMO of the acceptor. The expected structure due the intermolecular reaction between hexol and DNB is given in formula IV.

^{1}H-NMR ($CDCl_3$) for hexane-1,6-diol-1,3-dinitrobenzene, gave a signals at (Fig. 4): ^{1}H-NMR (DMSO-d_6, δ ppm): δ = 2.60 (t, 2H, (CH_2-OH), 2.65 (m, 2H, (CH_2CH_2-OH), 3.00 (m, 4H, ($CH_2CH_2CH_2CH_2$OH), 3.25 (m, 2H, (CH_2 CH_2 CH_2- CH_2CH_2OH), 3.25 (t, 2H, ($CH_2CH_2CH_2CH_2CH_2CH_2$OH), 3.34 (s (br), 1H, 1OH, hydrogen bonded), 4.02 (s , 1H, 1OH, non-hydrogen bonded), 7.74 (t appears s, H, Ar-H, C5), 8.52 (d, 2H, Ar-H, C4,C6), 8.88 (s, 1H, Ar-H, C2). The ^{1}H-NMR spectrum of hexol/DNB complex showed that the signals due to protons of CH_2 of the free aliphatic hexol were downfield shifted in the complex, referring to the formation of CT-complex between the electron poor DNB and the electron rich –OH of hexol.

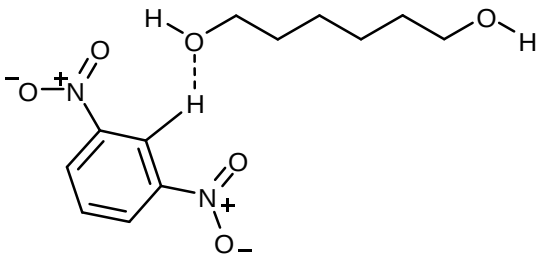

Formula IV. Suggested structure of [(hexol) (DNB)] complex.

3.4.4 [(hexol)(CLA)$_2$] complex

The appearance of a group of IR spectral bands in the spectrum of this CT-complex supports the conclusion that a deformation of the electronic environment of hexol is occurred by accepting protons from CLA. The IR spectrum of CT-complex is characterized by a band appearing in the region > 3400 cm^{-1}, which is not observed in the spectra of the free donor and acceptor. This band attributed to the stretching vibration of the intermolecular hydrogen bond from (–OH) group in CLA acceptor to the (–OH) group in hexol.

The reaction of hexol as donor with CLA as acceptor gave a new charge transfer complex named by hexane-1,6-diol-di(2,5-dichloro-3,6-dihydroxy-1,4-benzoquinone) (Formula V). ^{1}H-NMR (DMSO-d$_6$, δ ppm): δ = 1.42 (t, 4H, 2(C<u>H$_2$</u>CH$_2$CH$_2$-OH), 1.53 (m, 4H, 2(CH$_2$C<u>H$_2$</u>CH$_2$-OH)), 2.61 (t, 4H, 2(CH$_2$CH$_2$C<u>H$_2$</u>OH)), 2.83 (s, 2H, 2OH, 2(-CH$_2$-O<u>H</u>)), 5.74 (s, 2H, Ar-OH, hydrogen bonded), 8.67 (s, 2H, Ar-OH, phenolic protons). The ^{1}H-NMR showed broad signal at δ= 5.74 ppm which assigned to the involvement of -OH group in the formation of CT-complex between hexol and CLA. The hydrogen bonding of phenolic protons of CLA with the hexol hydroxyl groups increases the shielding effect by the lone pair of electrons of the oxygen atom of hexol, and this led to shifting their band to high filed, δ= 5.74 ppm and become more broad, while the non-hydrogen bonded phenolic protons appears at δ = 8.67 ppm due to the anisotropic effect of the benzene ring.

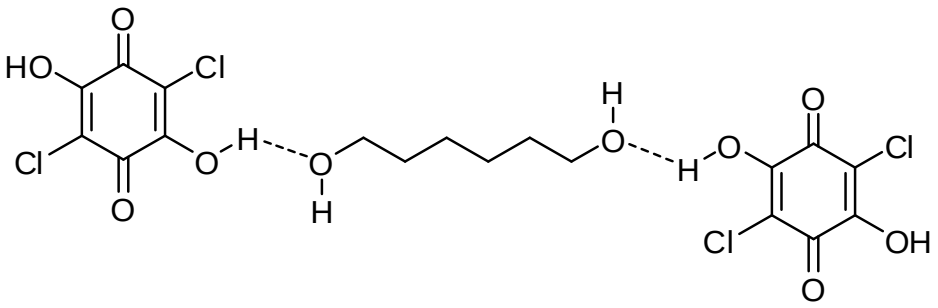

Formula V. Suggested structure of [(hexol) (CLA)$_2$] complex.

3.4.5 [(hexol)(CHL)$_2$] complex

The assignments data of hexol show that the intensive strong absorption band at 3392 cm^{-1} which characteristic of the ν(O-H) vibration of the hydroxyl group, was critically decreased in the

intensities in the CT-complex spectrum upon molecular complex formation. According to these observations, the suggested structure of [(hexol)$(CHL)_2$] complex was given in Formula VI.

For the reaction between hexol and CHL, the hexane-1,6-diol-di(2,3,5,6-tertachlorocyclohexa-2,5-diene-1,4-dione) compound is resulted. ^{1}H-NMR (DMSO-d_6, δ ppm): δ = 1.52 (t, 4H, 2($C\underline{H_2}CH_2CH_2$-OH), 1.69 (m appears singlet, 4H, 2($CH_2C\underline{H_2}CH_2$-OH)), 2.63 (s, 2H, 2OH, hydrogen bonded, 2(-CH_2-O$\underline{H}$)), 2.88 (t, 4H, 2($CH_2CH_2C\underline{H_2}OH)_2$). ^{1}H-NMR spectrum for this compound shows four main signals around 1.52, 1.69, 2.63 and 2.88 ppm, due to the three kinds of CH_2 protons of hexol and protons of OH group in hexol, respectively. All signals are downfield shifted compared to signals of free donor, referring to the formation of CT-complex. The ^{1}H- NMR spectroscopic data proved the formation of symmetrical compound with 8 different hydrogen protons, 6 for aliphatic CH_2 and 2 for OH of hexol.

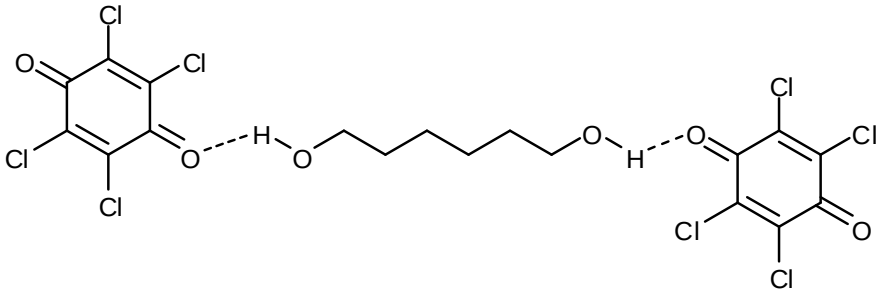

Formula VI. Suggested structure of [(hexol) $(CHL)_2$] complex.

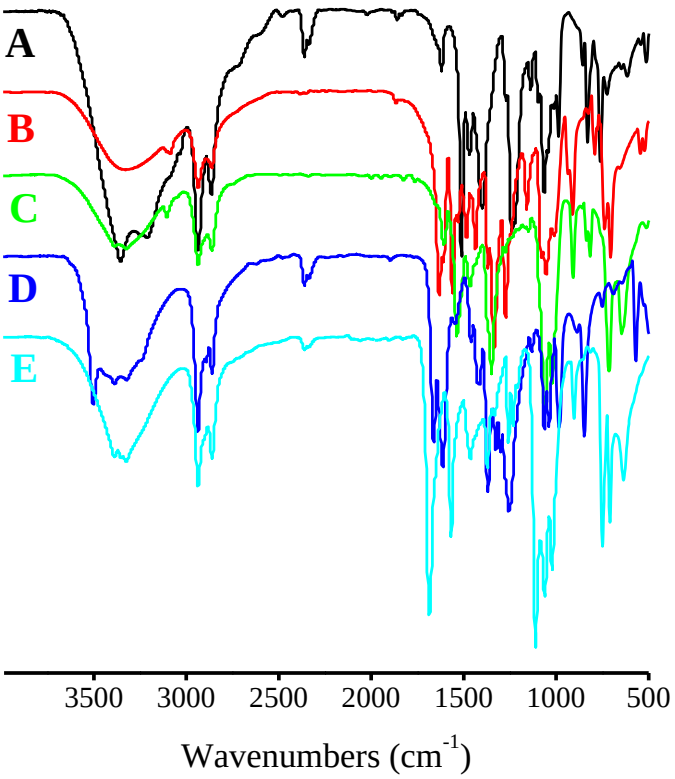

Figure 3. Infrared spectra of (A) hexol/$Q(OH)_2$, (B) hexol/PA, (C) hexol/DNB, (D) hexol/CLA and (E) hexol/CHL CT complexes.

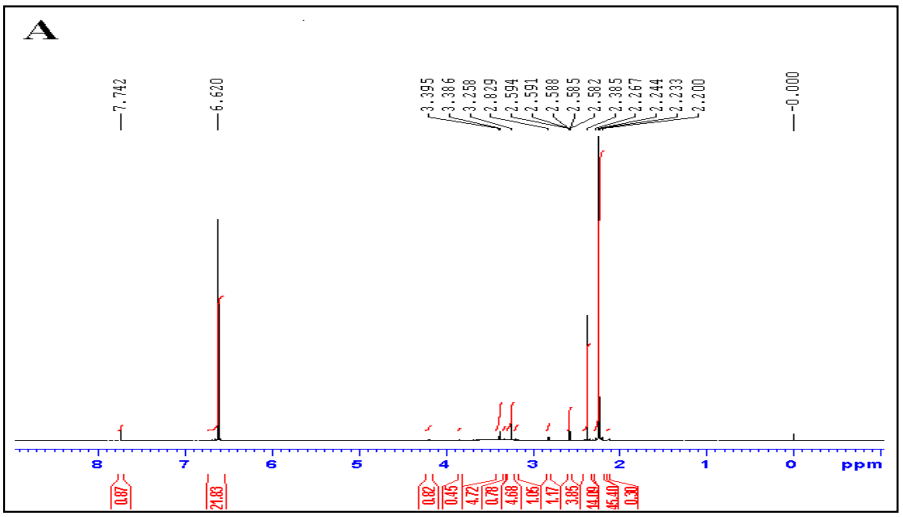
A
7.742
6.620
3.395
3.386
3.258
2.829
2.594
2.591
2.588
2.585
2.382
2.385
2.267
2.244
2.233
2.200
-0.000
ppm

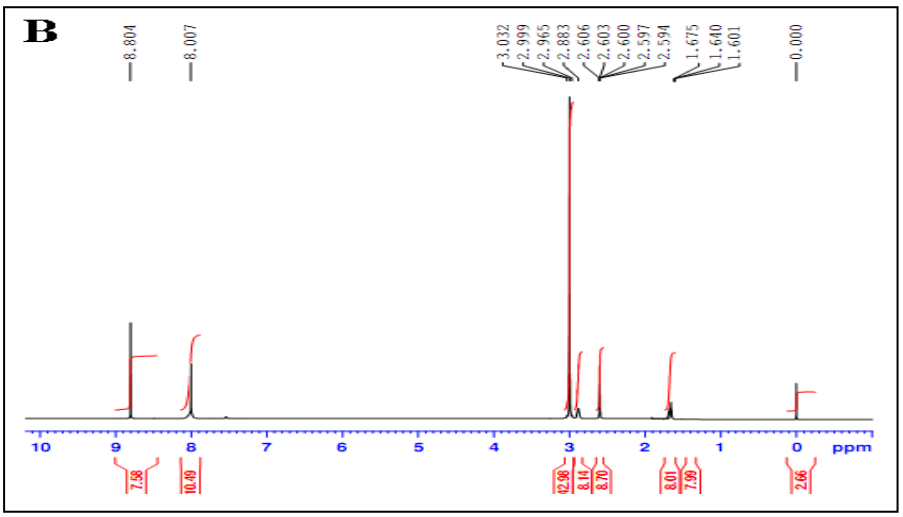
B
8.804
8.007
3.032
2.999
2.965
2.883
2.606
2.603
2.600
2.597
2.594
1.675
1.640
1.601
0.000
ppm

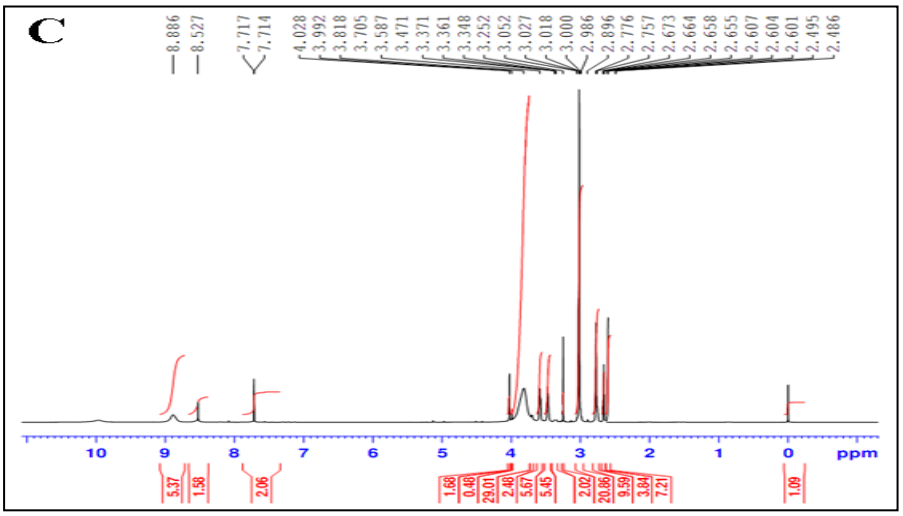
C
8.886
8.527
7.717
7.714
4.028
3.992
3.818
3.705
3.587
3.471
3.371
3.361
3.348
3.252
3.052
3.027
3.018
3.000
2.986
2.896
2.776
2.757
2.673
2.664
2.658
2.655
2.607
2.604
2.601
2.495
2.486
ppm

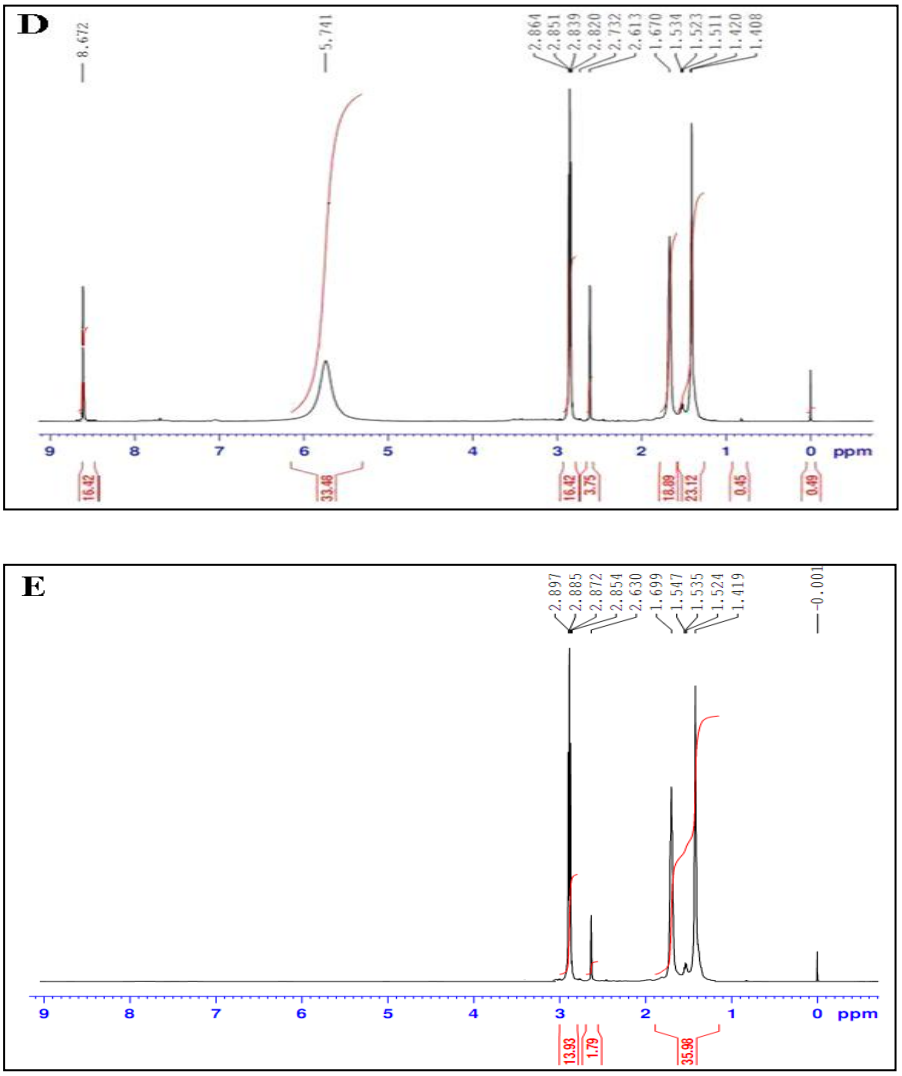

Figure 4. ^{1}H-NMR spectrum of (A) hexol/Q(OH)$_2$, (B) hexol/PA, (C) hexol/DNB, (D) hexol/CLA and (E) hexol/CHL complexes.

3.5 Thermogravimetric studies

The thermo gravimetric analysis give an idea about the thermal stabilities of the prepared charge transfer complexes and show the different in physical behavior between starting and resulting compounds [68]. The hexol CT-complexes are stable at room temperature and can be stored for several months without any changes. The obtained complexes were studied by thermogravimetric analysis from ambient temperature to 800 °C N_2 atmospheres. The TG curves were redrawn as mg mass loss versus temperature (TG). Typical TG curves of hexol CT-complexes are presented in Fig. 5, and the thermo analytical results are listed in Table 2. The overall loss of mass from the TG curves is 99.98% for [(hexol)(Q(OH)$_2$)], 99.94% for [(hexol)(PA)$_2$], 97.61% for [(hexol)(DNB)], 99.91% for [(hexol)(CLA)$_2$] and 95.03% for [(hexol)(CHL)$_2$].

The data obtained indicate that the [(hexol)(Q(OH)$_2$)] complex is thermally stable in the temperature range 25-130 °C. Decomposition of the complex start at ~130 °C and finished at ~300 °C, with maximum decomposition at 248 °C. The thermal decomposition of the complex occurs in one-

step within the range of 200-800 °C which attributed to the loss of $6C_2H_2$, $7H_2$ and 6CO molecules, representing a weight loss of obs.=99.98, cal.= 100.00%. The [(hexol)$(PA)_2$] complex beginning decomposed at ~70 °C in two definite decomposition steps (200 and 430 °C) within the temperature range 25-800 °C. The first decomposition step (obs. = 40.33%, calc. = 39.76%) within the temperature range 70-250 °C, may be attributed to the liberation of one molecule of PA. The second decomposition step existed within the temperature range 250-800 °C (obs. = 59.66%, calc. = 60.24%), which are reasonably by the loss of one molecule of PA and hexol molecule. The thermal analysis curve of [(hexol)(DNB)] complex show that decomposition takes places in one stage. This stage occurs at maximum temperature of 220 °C in the temperature range 250-800 corresponding to the formation of $4C_2H_2 + 5H_2 + 4CO + 2NO$. The curve of [(hexol)$(CLA)_2$] complex was thermally decomposed in nearly three decomposition steps within temperature range 25-800 °C. The first decomposition step (obs. = 32.56%, calc. = 32.84%) within temperature range 25-250 °C, may be assigned to the liberation of $2Cl_2$, $½O_2$ and H_2O molecules. The second decomposition step found within the temperature range 250-450 °C (obs. = 56.19%, calc. = 55.97%), which is assigned by the removal of $4C_2H_2$, $4H_2$, 5CO and $1.5O_2$ molecules with remaining five carbon atoms in the final step as a final residual. The CT-complex of hexol with CHL; [(hexol)$(CHL)_2$] complex, was degraded by two decomposition steps from 25-235 °C and 235-800 °C, with maximum temperature of 200 and 306 °C, respectively. The first decomposition step has a weight loss about 19.79% with librated of $1.5Cl_2$ and H_2O molecules. The last decomposition step has an extremely large scale of weight loss for about 75.66% due to libration of the rest of both donor and acceptor. Few carbon atoms remain as a final residual.

3.6 Kinetic thermodynamic studies

The kinetic studies on thermal process are expected to provide sufficient information regarding Arrhenius parameters viz. activation energy (E^*), frequency factor (A), enthalpy of activation (H^*), entropy of activation (S^*), free energy of activation (G^*). Two major different methods were applied for the evaluation of kinetic thermodynamic parameters, Coats-Redfern [69] and Horowitz-Metzger [70].

3.6.1 Coats-Redfern equation

The Coats-Redfern equation (10), which is atypical integral method, can be represented as:

$$\int_{0\to\infty} d\alpha/(1-\alpha)^n = (A/\varphi) \int_{T1\to T2} e^{-E^*/RT} dT \qquad (10)$$

For convenience of integration, the lower limit T_1 is usually taken as zero. This equation on integration gives:

$$\mathrm{Ln}[-\ln(1-\alpha)/ T^2] = - E^*/RT + \ln[AR/\varphi E^*] \qquad (11)$$

where α is the fraction of the sample decomposed at time T, T is the derivative peak temperature, A is frequency factor, R is the gas constant, E^* is the activation energy and φ is the linear heating rate. A plot of left-hand side (LHS) against $1/T$ was drawn. E^* is the energy of activation in KJ mol^{-1} and calculated from the slop and A in (s^{-1}) from the intercept. The entropy of activation ΔS^* in (JK^{-1} mol^{-1}) was calculated by using the equation:

$$\Delta S^* = R \ln (Ah/kT_s) \quad (12)$$

where k is the Boltzmann constant, h is the Plank's constant and T_s is the DTG peak temperature.

3.6.2 Horowitz-Metzger equation

The Horowitz-Metzger (Eg. 13) was written in the form as follows:

$$\log [\log (w_\alpha/w_\gamma)] = E^*\theta/2.303RT_s^2 - \log 2.303 \quad (13)$$

where $\theta = T - T_s$, $w_\gamma = w_\alpha - w$, w_α = mass loss at the completion of the reaction; w = mass loss up to time t.

The plot of Log[log (w_α/w_γ)] versus θ was drawn and found to be linear from the slope E^* was calculated. The pre-exponential factor, A, was calculated from the Eg. (14):

$$E^*\theta/RT_s^2 = A/ [\varphi \exp (-E^*/RT_s)] \quad (14)$$

From the TG curves, the activation energy, E^*, entropy of activations, ΔS^*, enthalpy activations, ΔH^*, and Gibbs free energy, ΔG^*, were calculate from;

$$\Delta H^* = E^* - RT \text{ and } \quad \Delta G^* = \Delta H^* - T\Delta S^*$$

The evaluated kinetic parameters for the first stages, using Coats-Redfern and Horowitz-Metzger equations, are listed in Table 3. The results show that the kinetic data obtained by the two methods are comparable and in harmony with each other. From Table 3, the following outcomes are draw:

1 Higher value of activation energy suggests the higher thermal stability. The complexes of CHL, DNB and $Q(OH)_2$ acceptors show higher values of activation energies, indicating higher thermal stability of these complexes.

2 The activation energy values (E^*) of hexol complexes arranged with order of thermal stability as: [(hexol)$(CHL)_2$] > [(hexol)(DNB)] > [(hexol)$(Q(OH)_2)$] > [(hexol)$(PA)_2$] = [(hexol)$(CLA)_2$].

3 The higher values of (E^*) and lower values of (A) favor the reaction to proceed slower than normal [71]. This can be seen in case of hexol/PA and hexol/CLA complexes.

4 The satisfactory values of correlation coefficients of the Arrhenius plots of the thermal decomposition steps were found to be (r ~ 1) in all cases indicate good fit with linear function and reasonable agreement between experimental data and the values of kinetic parameters.

5 It is clear that the thermal decomposition process of all hexol complexes is non-spontaneous, i.e., the complexes are thermally stable.

3.7 Antimicrobial activities

Applying the disc diffusion method, all of the newly synthesized hexol complexes were screened in vitro for antibacterial and antifungal activity. The activity was determined against four bacterial species, two Gram (+); *Staphylococcus aureus* (*S. aureus*) and *Bacillus subtilis*, and two Gram (-); *Escherichia coli* (*E. coli*) and *Pseudomonas aeuroginosa* (*P. aeuroginosa*). The antifungal screening was studied against two species, *Aspergillus flavus* and *Candida albicans*. The activity was performed by measuring the inhibition zone diameter values (mm) of the investigated complexes against microorganisms and the screening results obtained are listed in Table 4, and statistically presented in Figures 6 and 7. A comparative study of hexol complexes showed that hexol/$Q(OH)_2$ and hexol/CHL complexes exhibit an antibacterial activity against all Gram-positive and Gram-negative bacteria species than other complexes. The results show that only hexol/$Q(OH)_2$ and hexol/PA complexes exhibit good antifungal activity against *Candida albicans*. All the five complexes exhibited no inhibitory activates against *Aspergillus flavus* species.

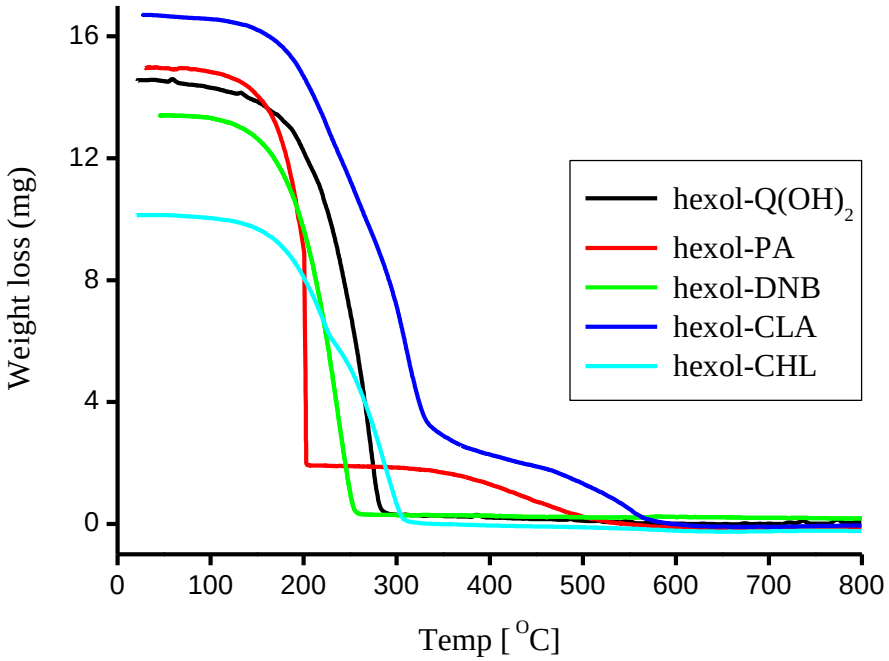

Figure 5. TG curves of hexol CT-complexes.

Table 2. Thermo analytical results for the hexol CT-complexes**.**

Samples	Stage	TG range (°C)	Max.temp. (°C)	Weight loss (%)		Evolved moiety
				Found	Calc.	
hexol/Q(OH)$_2$ ($C_{18}H_{26}O_6$)	I	25-800	248	99.98	100	$6C_2H_2 + 7H_2 + 6CO$
hexol/PA ($C_{18}H_{20}O_{16}N_6$)	I	25-250	200	40.33	39.76	PA
	II	250-800	430	59.66	60.24	PA, Hexol
hexol/DNB ($C_{12}H_{18}O_6N_2$)	I	25-800	220	98.66	100	$4C_2H_2 + 5H_2 + 4CO + 2NO$
hexol/CLA ($C_{18}H_{18}O_{10}Cl_4$)	I	25-250	200	32.56	32.84	$2Cl_2 + ½O_2 + H_2O$
	II	250-450	300	56.19	55.97	$4C_2H_2 + 4H_2 + 5CO + 1.5O_2$
	III	450-800	510	11.25	11.19	5C
hexol/CHL ($C_{18}H_{14}O_6Cl_8$)	I	25-235	200	19.79	20.41	$1.5Cl_2 + H_2O$
	II	235-800	306	76.16	75.66	CHL, $5C_2H_2 + Cl_2 + H_2O + O_2$
	Residue			4.05	3.94	2C

Table 3. Kinetic parameters determined using the Coats-Redfern (CR) and Horowitz-Metzger ((HM)**.**

Complexes	Method	Parameters [a]				
		E^*	A	ΔS^*	ΔH^*	ΔG^*
[(hexol)(Q(OH)$_2$)$_2$]	CR	1.65×10^5	9.63×10^{13}	-1.65×10^2	1.63×10^5	1.50×10^5
	HM	1.87×10^5	10.81×10^{15}	-1.87×10^2	1.55×10^5	1.46×10^5
[(hexol)(PA)$_2$]	CR	3.22×10^4	6.93×10^3	-1.83×10^2	2.90×10^4	9.43×10^4
	HM	3.51×10^4	7.87×10^5	-1.81×10^2	2.67×10^4	9.31×10^4
[(hexol)(DNB)]	CR	1.88×10^5	2.67×10^{21}	-1.64×10^2	1.42×10^5	9.11×10^4
	HM	1.94×10^5	2.77×10^{23}	-1.51×10^2	1.46×10^5	9.69×10^4
[(hexol)(CLA)$_2$]	CR	3.22×10^4	2.33×10^3	-1.44×10^2	3.22×10^4	9.22×10^4
	HM	3.17×10^4	2.91×10^5	-1.36×10^2	3.16×10^4	10.34×10^4
[(hexol)(CHL)$_2$]	CR	2.22×10^5	1.33×10^{17}	-1.76×10^2	2.19×10^5	1.66×10^5
	HM	2.35×10^5	1.46×10^{15}	-1.66×10^2	2.11×10^5	1.51×10^5

[a] Units of parameters: E in kJ mol^{-1}, A in s^{-1}, ΔS in J mol^{-1}K^{-1}, ΔH and ΔG in kJ mol^{-1}.

Table 4. The inhibition diameter zone values (mm) for hexol CT-complexes.

Sample	Inhibition zone diameter (mm/mg sample)					
	Bacteria				Fungi	
	Bacillus subtilis, (G^+) [a]	*Escherichia coli*, (G^-)	*Pseudomonas aeuroginosa*, (G^-)	*Staphylococcus aureus*, (G^+)	*Aspergillus flavus*	*Candida albicans*
Control: DMSO	0.0	0.0	0.0	0.0	0.0	0.0
Tetracycline	34.0	32.0	34.0	30.0	-	-
Amphotericin B	-	-	-	-	18.0	19.0
hexol/Q(OH)$_2$	9.0	9.0	12.0	12.0	0.0	14.0
hexol/PA	9.0	0.0	0.0	0.0	0.0	10.0
hexol/DNB	0.0	9.0	0.0	9.0	0.0	0.0
hexol/CLA	0.0	0.0	0.0	0.0	0.0	0.0
hexol/CHL	10.0	11.0	12.0	9.0	0.0	0.0

[a] G: Gram reaction.

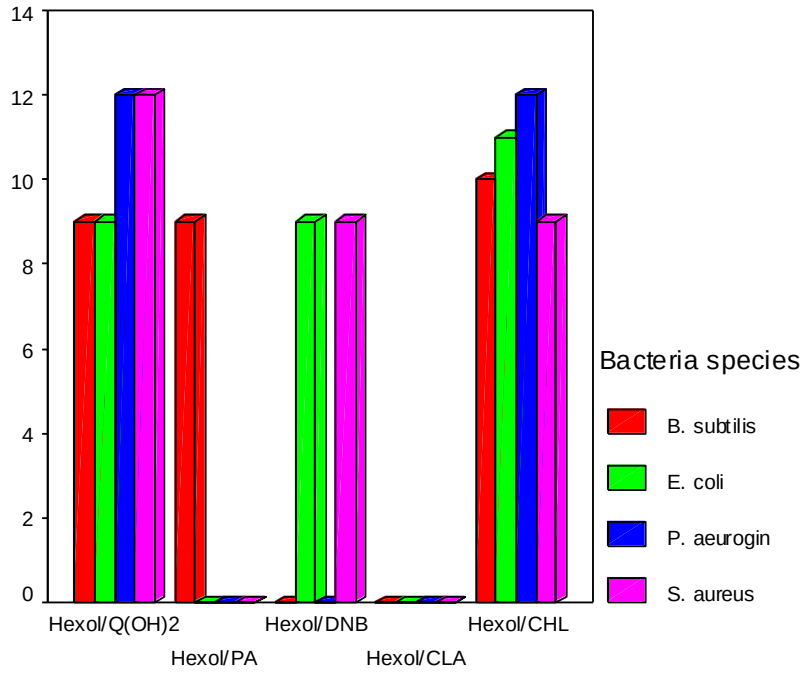

Figure 6. Statistical representation for antibacterial activity of hexol complexes.

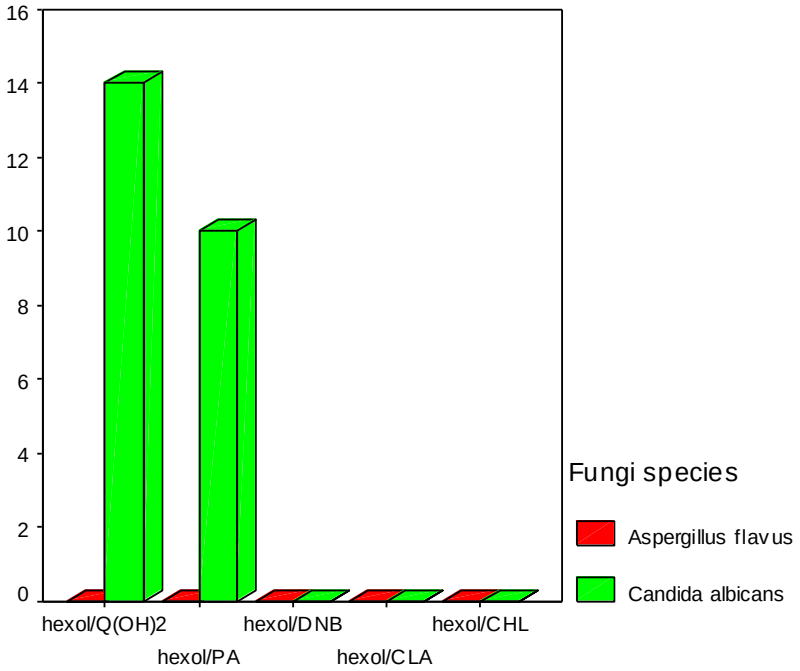

Figure 7. Statistical representation for antifungal activity of hexol complexes.

3.8 HOMO and LUMO analysis

Molecular orbital and their properties like energy are very useful to the physicists and chemists and their frontier electron density used for predicting the most reactive position in π-electron system

and also explained several types of reaction in conjugated system [72]. The electronic absorption corresponds to the transition from the ground to the first excited state is mainly described by on electron excitation from the highest occupied molecular orbital (HOMO) to the lowest unoccupied molecular orbital (LUMO) [73]. Moreover, the Eigen values of highest occupied molecular orbitals – HOMOs (π donor) and lowest unoccupied molecular orbitals – LUMOs (π acceptor) and their energy gap reflect the chemical activity [74]. Recently, the energy gap between HOMO and LUMO has been used to prove the bioactivity from intra-molecular charge transfer (ICT) [75,76].

Computational analysis of energy levels of HOMO and LUMO orbitals was calculated and the frontier orbitals (HOMO, LUMO) of free hexol donor and CT-complexes are plotted in Fig. 8. The HOMO, LUMO and the results of the energy gap values are reported in Table 5. Hexol/DNB and hexol/CLA complexes present a decreased HOMO-LUMO energy gap compared to $Q(OH)_2$, PA and CHL complexes, and this is due to a strong increase of HOMO energy, while LUMO energy increases slightly. The reduced HOMO-LUMO energy gap can be read as a prediction of enhanced reactivity, hence reduced stability, of the DNB and CLA complexes. On the other hand, the hexol/PA and hexol/$Q(OH)_2$ complexes have high-energy gap equal to 16.4 and 7.3 eV, respectively, which are the more stable hexol complexes. The order of stability can be summarized as; PA > $Q(OH)_2$ > CHL > DNB > CLA.

It is clearly shown from antimicrobial results and energy gap values that, the hexol complexes which have high energy gap values exhibit an antibacterial activity against all bacteria species under investigation, and only hexol/$Q(OH)_2$ and hexol/PA complexes, which possess highest energy gap value exhibit good antifungal activity against *Candida albicans*. The obtained results reveal that the energy gap reflects the chemical and biological activity of the charge transfer complex.

Table 5. HOMO, LUMO and energy gap values of hexol and CT-complexes in eV.

Compound	HOMO	LUMO	Energy gap
hexol/$Q(OH)_2$	-1.328	-8.674	7.346
hexol/PA	205.593	189.208	16.385
hexol/DNB	-9.177	-8.855	-0.322
hexol/CLA	-9.043	-7.406	-1.637
hexol/CHL	-2.390	-7.406	5.016

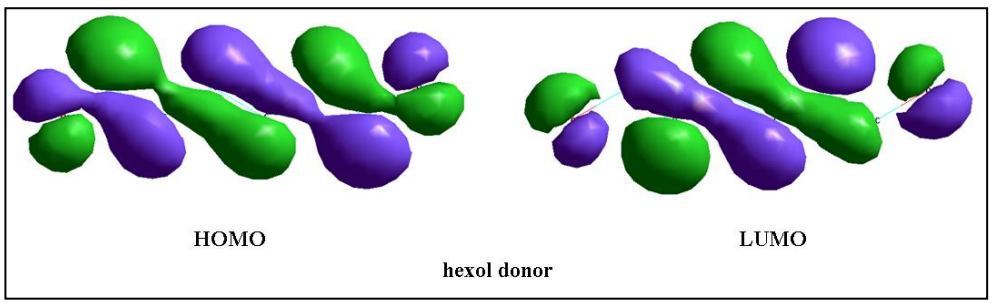

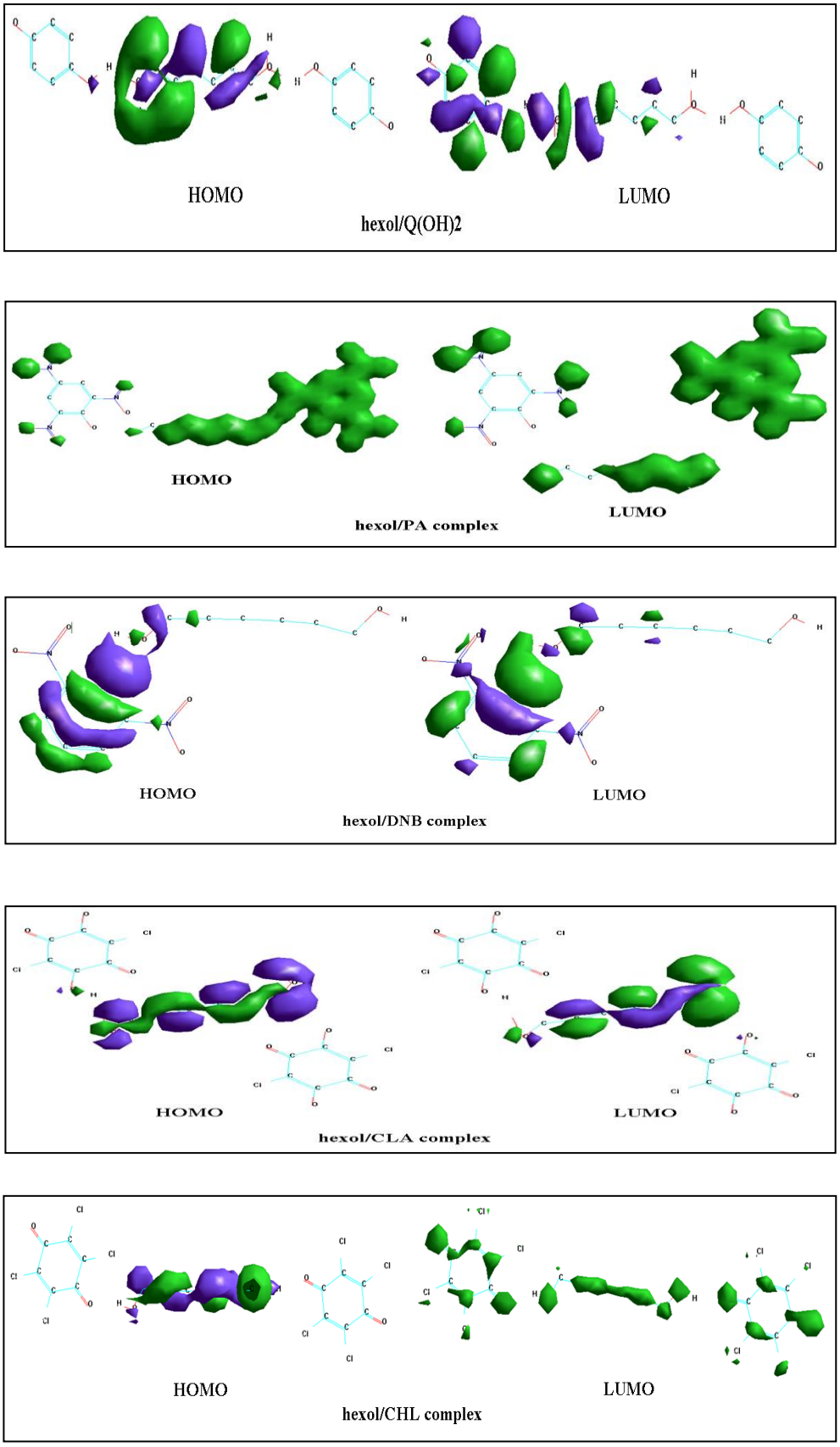

Figure 8. HOMO and LUMO plots of free hexol donor and CT-complexes.

References

1. R.S. Mulliken, *J. Am. Chem. Soc.* 72 (1950) 4493.
2. R.S. Mulliken, W.B. Pearson, Molecular Complexes, Wiley Publishers, New York, 1969.
3. R. Foster, Charge Transfer Complexes, Academic press, London, 1969.
4. R.S. Mulliken, *J. Am. Chem. Soc.* 74 (1952) 811.
5. R.S. Mulliken, *J. Phys. Chem.* 56 (1952) 801.
6. D.K. Roy, A. Saha, A.K. Mukherjee, *Spectrochim. Acta A 61* (2005) 2017.
7. A.M. Slifkin, Charge-transfer Interaction of Biomolecules, Academic Press, New York, 1971.
8. A. Dozal, H. Keyzer, H.K. Kim, W.W. Wang, *Int. J. Antimicrob. Agent 14* (2000) 261.
9. A. Korolkovas, Essentials of Medical Chemistry, 2nd ed., Wiley, New York, 1998 (Chapter 3).
10. F.M. Abou Attia, *Farmaco 55* (2000) 659.
11. K. Basavaiah, *Farmaco 59* (2004) 315.
12. G.A. Saleh, H.F. Askal, M.F. Radwan, M.A. Omar, *Talanta 54* (6) (2001) 1205.
13. H. Salem, J. Pharm. Biomed. Anal. 29 (3) (2002) 527.
14. M. Pandeeswaran, E.H. El-Mossalamy, K.P. Elango, *Int. J. Chem. Kinet. 41 (*2009) 787.
15. M. Pandeeswaran, K.P. Elango, *Spectrochim. Acta A 75* (2010) 1462.
16. M.S. Refat, A.M. El-Didamony, *Spectrochim. Acta A 65* (3-4) (2006) 732.
17. M.S. Refat, G.G. Mohamed, A. Fathi, *Bull. Korean Chem. Soc. 31* (6) (2010) 1535.
18. M.S. Refat, S.A. El-Korashy, I.M. El-Deen, S.M. El-Sayed, *J. Mol. Struct. 980* (2010) 124.
19. A.M.A. Adam, M. Salman, T. Sharshar, M.S. Refat, *Int. J. Electrochem. Sci. 8* (2013) 1274.
20. M.S. Refat, O.B. Ibrahim, H. Al-Didamony, K.M. Abou El-Nour, L. El-Zayat, *J. Saudi Chem. Soc.*, in press, doi: 10.1016/j.jscs.2010.12.008.
21. M.S. Refat, *J. Mol. Struct. 985* (2011) 380.
22. M.S. Refat, W.F. El-Hawary, M.A.A. Moussa, *Spectrochim. Acta A 78* (2011) 1356.
23. M.S. Refat, A. Elfalaky, E. Elesh, *J. Mol. Struct. 990* (2011) 217.
24. M.S. Refat, S.A. Sadeek, H.M. Khater, *Spectrochim. Acta A 64* (3) (2006) 778.
25. M.S. Refat, I. Grabchev, J.-M. Chovelon, G. Ivanova, *Spectrochim. Acta A 64* (2) (2006) 435.
26. M.S. Refat, H. Al-Didamony, L.A. El-Zayat, Can. *J. Anal. Sci. Spec. 51* (3) (2006) 147.
27. M.S. Refat, H.M.A. Killa, I. Grabchev, M.Y. El-Sayed, *Spectrochim. Acta A 68* (1) (2007) 123.
28. M.S. Refat, H.A. Ahmed, Ivo. Grabchev, L.A. El-Zayat, *Spectrochim. Acta A 70* (4) (2008) 907.
29. M.S. Refat, H.M.A. Killa, I. Grabchev, M.Y. El-Sayed, *The Canadian Journal of Analytical Science and Spectroscopy 52* (2) (2007) 75.
30. M.S. Refat, L.A. El-Zayat, Okan Zafer Yesilel, *Spectrochimica Acta Part A* 75 (2010) 745.
31. M.S. Refat, H.A. Saad, A.M.A. Adam, *J. Mol. Struct. 995* (2011) 116.
32. F.P. Fla, J. Palou, R. Valero, C.D. Hall, P. Speers, *J. Chem. Soc., Perkin Trans. 2* (1991) 1925.
33. F. Yakuphanoglu, M. Arslan, *Solid State Commun. 132* (2004) 229.
34. F. Yakuphanoglu, M. Arslan, *Opt. Mater. 27* (2004) 29.
35. F. Yakuphanoglu, M. Arslan, M. Kucukislamoglu, M. Zengin, *Sol. Energy 79* (2005) 96.
36. B. Chakraborty, A.S. Mukherjee, B.K. Seal, *Spectrochim. Acta A 57* (2001) 223.
37. M. Krishnamurthy, K. Surendrababu, U. Muralikrishna, *Indian J. Chem. 27 A* (1988) 669.
38. S.M. Andrade, S.M.B. Costa, R. Pansu, *J. Colloid Interface Sci. 226* (2000) 260.
39. R. Dabestani, K.J. Reszka, M. E. Sigman, *J. Photochem. Photobiol. A 117* (1998) 223.
40. R. Jakubiak, Z. Bao, L. Rothberg, *Synth. Met. 114* (2000) 61.
41. K. Takahasi, K. Horino, T. Komura, K. Murata, *Bull. Chem. Soc. Jpn. 66* (1993) 733.
42. A. Eychmuller, A.L. Rogach, *Pure Appl. Chem. 72* (2000) 179.
43. K. Brueggermann, R.S. Czernuszewicz, J.K. Kochi, *J. Phys. Chem. 96* (1992) 4405.
44. S.K. Das, G. Krishnamoorthy, S.K. Dofra, *Can. J. Chem. 78* (2000) 191.
45. G. Jones, J.A.C. Jimenez, *Tetrahedron Lett. 40* (1999) 8551.
46. G. Smith, D.E. Lynch, K.A. Byriel, C.H.L. Kennard, *J. Chem. Crystallogr. 27* (1997) 307.

47. G. Smith, D.E. Lynch, R.C. Bott, *Aust. J. Chem. 51* (1998) 159.
48. G. Smith, R.C. Bott, A.D. Rae, A. C. Willis, *Aust. J. Chem. 53* (2000) 531.
49. D.A. Skoog, Principle of Instrumental Analysis, third ed., Saunders, New York, USA, 1985 (Chapter 7).
50. H.A. Benesi, J.H. Hildebrand, *J. Am. Chem. Soc. 71* (1949) 2703.
51. R. Abu-Eittah, F. Al-Sugeir, *Can. J. Chem. 54* (1976) 3705.
52. A.W. Bauer, W.M. Kirby, C. Sherris, M. Turck, *American Journal of Clinical Pathology 45* (1966) 493.
53. M.A. Pfaller, L. Burmeister, M.A. Bartlett, M.G. Rinaldi, *J. Clin. Microbiol. 26* (1988) 1437.
54. D.J. Beecher, A.C. Wong, *Applied and Environmental Microbiology 60* (1994) 1646.
55. National Committee for Clinical Laboratory Standards. Reference Method for Broth Dilution Antifungal Susceptibility Testing of Conidium-Forming Filamentous Fungi: Proposed Standard M38-A. NCCLS, Wayne, PA, USA (2002).
56. National Committee for Clinical Laboratory Standards. Method for Antifungal Disk Diffusion Susceptibility Testing of Yeast: Proposed Guideline M44-P. NCCLS, Wayne, PA, USA (2003).
57. National Committee for Clinical Laboratory Standards. Methods for Antimicrobial Susceptibility Testing of Anaerobic Bacteria: Approved Standard M11-A3. NCCLS, Wayne, PA, USA (1993).
58. H. Tsubomura, R.P. Lang, J. Am. Chem. Soc. 83 (1961) 2085.
59. R. Rathone, S.V. Lindeman, J.K. Kochi, *J. Am. Chem. Soc. 119* (1997) 9393.
60. G. Aloisi, S. Pignataro, *J. Chem. Soc. Faraday Trans. 69* (1972) 534.
61. G. Briegleb, J. Czekalla, Z. Physikchem, *Frankfurt 24* (1960) 237.
62. G. Briegleb, Z. Angew. Chem. 72 (1960) 401, *Z. Angew. Chem. 76* (1964) 326.
63. A.N. Martin, J. Swarbrick, A. Cammarata, Physical Pharmacy, 3rd ed., Lee and Febiger, Philadelphia, PA, 1969, p. 344.
64. A.S.M. Hossan, H.M. Abou-Melha, M.S. Refat, *Spectrochim. Acta A 79* (2011) 583.
65. A.M.A. Adam, Spectrochim. Acta A 104 (2013) 1.
66. R. Bharathikannan, A. Chandramohan, M.A. Kandhaswamy, J. Chandrasekaran, R. Renganathan, V. Kandavelu, *Cryst. Res. Technol. 43* (6) (2008) 683.
67. A.A. Adam, *J. Mol. Struct. 1030* (2012) 26.
68. M.S. Refat, H.A. Saad, A.A. Adam, *Spectrochim. Acta A 79* (2011) 672.
69. A.W. Coats, J.P. Redfern, Nature (London) 201 (1964) 68.
70. H.H. Horowitz, G. Metzger, Anal. Chem. 35 (1963) 1464.
71. N. Sharma, Archana, M. Thakur, S.S. Bhatt, S.C. Chaudhry, *J. Chem. Sci. 119* (4) (2007) 311.
72. K. Fukui, T. Yonezawa, H. Shingu, *J. Chem. Phys. 20* (1952) 722.
73. V. Krishnakumar, D. Barathi, R. Mathammal, *Spectrochim. Acta A 86* (2012) 196.
74. R. John Xavier, E. Gobinath, *Spectrochim. Acta A 86* (2012) 242.
75. L. Padmaja, C. Ravi Kumar, D. Sajan, I. Hubert Joe, V.S. Jayakumar, G.R. Pettit, *J. Raman Spectrosc. 40* (2009) 419.
76. S. Sagdinc, H. Pir, *Spectrochim. Acta A 73* (2009) 181.